

Compressive Behaviour of Metal Matrix Syntactic Foams

Imre Norbert Orbulov

Department of Materials Science and Engineering, Budapest University of Technology and Economics, Bertalan Lajos utca 7, H-1111, Budapest, Hungary, orbulov@eik.bme.hu

János Ginsztler

Research Group for Metals Technology of the Hungarian Academy of Sciences, Bertalan Lajos utca 7, H-1111, Budapest, Hungary, jginsztler@mti.bme.hu

Abstract: The compressive behaviour of three different metal matrix syntactic foams (MMSFs) was investigated. The results showed that the engineering factors such as the size of the used hollow spheres, the aspect ratio (height / diameter ratio) of the specimens and the temperature of the tests have significant effects on the compressive strength and properties. The smaller microballoons with thinner wall ensured higher compressive strength due to their more flawless microstructure and better mechanical stability. The higher aspect ratio of the specimens resulted in worse compressive characteristics (lower strength, lower specific energy consuming capacity). The elevated temperature tests revealed ~30% drop in the compressive strength. However, the strength remained high enough for structural applications; therefore MMSFs are good choices for light structural parts working at elevated or room temperature. The proper size selection of the reinforcing hollow spheres ensures potential for tailoring the compressive characteristics of MMSFs.

Keywords: metal matrix composite; syntactic foams; metallic foams; compressive properties

1 Introduction

Nowadays metallic foams have become more and more important, and this is confirmed by the increasing number of papers published on this topic. The 'conventional' metallic foams, which consist of a metal structure, a gas phase and stabilising particles, have been written about widely in the literature thanks to their potential application possibilities as automotive parts, energy absorbers or blast and collision damping elements in buildings or vehicles, etc. However, there are

still existing problems, for example in the foaming process [1, 2]. The metallic foams have a special class, namely metal matrix syntactic foams (MMSFs). In MMSFs, the porosity is ensured by the incorporation of ceramic microballoons [3, 4]. The microballoons are commercially available and they contain mainly various oxide ceramics [5, 6]. The quality of the microballoons (uniform wall thickness and flawless wall) has a strong effect on the mechanical and other properties of the foams. The MMSFs have numerous perspective applications (covers, hulls, walls, castings, or in the automotive industry sectors) because of their high energy absorbing and damping capability and due to their low density [7].

The MMSFs can be produced by pressure infiltration or by stir casting; both ways are common in the literature. The main mechanical load mode of MMSFs is compression; therefore, the compression characteristics have been investigated in some aspects. Palmer *et al.* studied the pressure infiltration process and mechanical behaviour of various microballoon and metal matrix combinations. Compressive stress-strain data were gathered for foams prepared from combinations of Al1350, Al5083 and Al6061 alloys for both 45 μm and 270 μm spheres [8]. Balch *et al.* fabricated aluminium matrix MMSFs by liquid metal infiltration of commercially pure (cp-Al) and Al7075 aluminium. The cp-Al foam exhibited peak strengths in compression of over 100 MPa, but the Al7075 matrix foams had significantly higher peak strengths, up to 230 MPa [9, 10]. Rohatgi *et al.* investigated the pressure infiltration technique of nickel coated and uncoated microballoons. In their other work, loose beds of microballoons (cenospheres) were pressure infiltrated with A356 alloy melt to fabricate MMSFs. The processing variables included melt temperature, gas pressure and the size of microballoons. The effect of these processing variables on the microstructure and compressive properties of the synthesized composites was characterized [11, 12]. Kiser *et al.* performed investigations on the mechanical response of MMSFs under both uniaxial compression and constrained die compression loadings. The key material parameters that varied were the matrix strength and the ratio of the wall thickness to radius of the microballoons. They observed that the energy absorption capacity was extremely high in comparison with values that are typical of 'conventional' metal foams [13]. Wu *et al.* established a new method to predict the compressive strength of MMSFs, showing the relation between the relative wall thickness of the microballoons and the compressive strength of such foams. The deformation mechanisms of syntactic foams was also discussed [14]. Tao *et al.* investigated the mechanical properties of MMSFs with monomodal and bimodal distribution of microballoons. The bimodal foams have the advantages of a flat plateau regime, high plateau stress, lower density and good ductility. In the next step, Al matrix MMSFs with additional Al particles embedded were fabricated by pressure infiltration. With the introduction of Al particles, the ductility of the syntactic foams was significantly increased, and the compressive strength also increased by up to 30% [15, 16]. Zhang *et al.* manufactured aluminium matrix MMSFs with low-cost porous ceramic spheres of diameters between 0.25 and 4 mm by pressure infiltration casting. The mechanical response of the syntactic

foams with different sphere sizes and densities under static and dynamic conditions was investigated. They found that the plateau strength, and thus the amount of energy absorption of the syntactic foam, was largely determined by the volume fraction of Al and to a lesser extent by the mechanical properties of the ceramic spheres in the foam [17]. In the works of Mondal et al., microballoons in the range of 30–50 vol% were used as space holders for making syntactic aluminium foam using a stir-casting technique. The synthesized MMSF was characterized in terms of microstructures, hardness and compressive deformation behaviour. The plateau stress of these MMSFs is considerably higher than those of conventional aluminium foams. The dry sliding wear behaviour of MMSFs has also been studied using a pin-on-disc apparatus [18, 19]. Rabiei and O'Neill produced MMSFs using gravity casting techniques. The foam was comprised of steel hollow spheres packed into a random dense arrangement, with the interstitial space between spheres infiltrated with a casting aluminium alloy. The composite foam developed in the study displayed superior compressive strength and energy absorption capacity [20]. Ramachandra and Radhakrishna synthesized aluminium based MMSFs containing up to 15 wt% of microballoons by the stir casting method. Properties like density, hardness, microhardness, ductility and ultimate tensile strength were investigated. The MMSFs produced were also subjected to corrosion, dry sliding wear and slurry erosive wear tests. The addition of microballoons reduced the density of composites while increasing some of their mechanical properties. The results of wear studies have shown that the resistance to wear increased with an increase in the percentage of microballoons [21, 22]. In the work of Couteau and Dunand, aluminium MMSFs with densities of 1.2-1.5 g/cm³ were deformed at 500°C under constant uniaxial compressive stresses ranging from 5 to 14 MPa. The foam's creep behaviour was characterized by a short primary stage and a long secondary stage where the strain rate was constant and minimum [23]. The microballoons in MMSFs work as stress concentrators and have influence on the crack propagation in materials [24].

Most of the MMSFs are produced by pressure infiltration; therefore, the infiltration parameters (like required threshold pressure) have also been studied. Trumble presented an analysis of spontaneous infiltration to model non-cylindrical pores. [25]. Bárczy and Kaptay developed a new infiltration model for 'closely packed equal sphere - CPES' structure. In their study the threshold pressure, the threshold contact angle and the equilibrium height of penetration were determined. All these parameters are significantly different from those obtained from the traditional capillary penetration model, but similar to the Carman model. The experiments demonstrated the reliability of the theoretical results [26]. Asthana et al. also overviewed some fundamental materials phenomena relevant to the infiltration processing of metal-matrix composites. They stated that the lack of a comprehensive theoretical framework required further research to be done [27].

The aim of this paper is to extend the knowledge regarding MMSFs by analysing the effects of the microballoon size, the elevated test temperature and the effects of the aspect ratio (height / diameter ratio) of compression specimens.

2 Investigated Materials

Overall three types of MMSFs were produced by pressure infiltration from the combination of technical purity aluminium (Al99.5) and three ceramic microballoons (designated by SL150, SL300 and Globocer). The chemical composition of the matrix material is listed in Table 1.

Table 1
Chemical composition of Al99.5 material

Matrix	Composition (wt%)								
	Al	Si	Fe	Cu	Mn	Mg	Zn	V	Ti
Al99.5	99.5	0.25	0.4	0.05	0.05	0.05	0.05	0.05	0.03

The SL150 and SL300 microballoons were provided by Envirospheres Pty Ltd [6], while the Globocer type hollow spheres were shipped by Hollomet GmbH [28]. The main differences between the three types are in the average diameter, density and wall thickness. Their main parameters are summarized in Table 2.

Table 2
Morphological properties and phase constitution of the applied hollow ceramic spheres

Type	Density at 64 vol% (gcm ⁻³)	Average		Al ₂ O ₃	SiO ₂	Mullite	Quartz
		diameter (µm)	thickness (µm)				
SL150	0.576	100	3.69				
SL300	0.691	150	6.75	30-35	45-50	15-20	0-5
Globocer	0.816	1450	58				

The MMSFs were produced by pressure infiltration in a special infiltration chamber (Fig. 1). In the first step, the microballoons were poured into a mould to the half and they were densified by gentle tapping and knocking to get a randomly closed pack structure (RCPS). The maximal volume fraction that can be reached with quasi-equal diameter spheres is 64 vol%, as is published in [29]. After this, a layer of alumina mat separator was placed on the top of the microballoons and a block of matrix material was put on the mat. The mould was situated into the infiltration chamber, the chamber was closed and the whole system was evacuated by a vacuum pump (rough vacuum). Proper heating was ensured by three heating zones and the temperatures of the matrix block and the microballoons were

continuously monitored by two thermocouples. After the melting of the matrix, the vacuum pump was switched off and argon gas was let into the chamber at a previously set pressure. Due to this, a pressure difference was built up between the mould (vacuum) and the chamber (argon pressure). This pressure difference forced the molten metal to infiltrate the space between the microballoons. After solidification the mould was removed and cooled to room temperature.

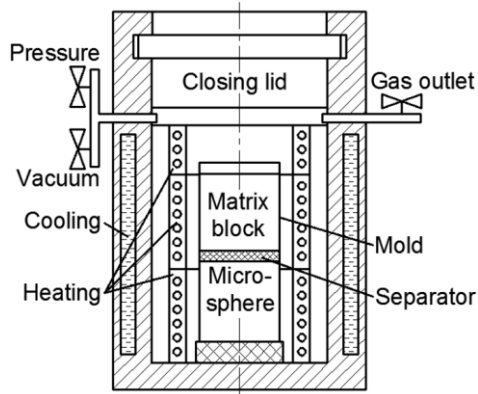


Figure 1

Schematic sketch of the infiltration chamber

Then the complete MMSF block ($\sim 40 \times 60 \times 180$ mm) could be removed from the mould. For further details about the production process, please refer to [4]. The blocks were designated by their constituents: for example, Al99.5-SL150 stands for an MMSF block with Al99.5 matrix and with ~ 64 vol% SL150 microballoons. The main physical properties, such as density, porosity, are presented in Table 3.

Table 3

Density and porosity values of the prepared MMSFs

Specimen	Density (g/cm^3)		Porosity (%)		
	Theoretical	Measured	Microballoon	Matrix	Total
Al99.5-SL150	1.34	1.43	50.9	-6.3	44.7
Al99.5-SL300	1.41	1.52	48.2	-7.2	41.0
Al99.5-Globocer	1.53	1.49	45.0	2.6	47.6

The theoretical density and microballoon-porosity (the porosity ensured by the hollow spheres) were calculated from the average geometrical parameters of the microballoons. The matrix porosities (the volume of the pores in the matrix material divided by the volume of the whole specimen) were calculated as the difference between the theoretical and measured density divided by the theoretical density. The negative matrix porosity refers to the infiltrated microballoons (the microballoon-porosity should be decreased). The values of the matrix porosity always remained below 7.2%, so the infiltration can be qualified as a suitable one.

3 Experiments

The main loading mode of foam materials is the compression; therefore compression tests were performed on the cylindrical specimens. The diameter (D) of the specimens was 14 mm and the height (H) of the specimens was 14, 21 and 28 mm (aspect ratio (H/D) 1, 1.5 and 2 respectively). The compression tests were performed on a MTS 810 type universal testing machine in a four column tool at room temperature. The surfaces of the tool were grinded and polished. The specimens and the tool were lubricated with anti-seize material. The test speed was 0.15 mm/s, which ensured quasi-static compression. Six specimens were compressed at room temperature and at elevated (220 °C) temperature until 50% engineering strain from each MMSF type to get representative results. Overall 36 specimens were compressed (at room temperature: 6 pcs Al99.5-SL150, 6 pcs Al99.5-SL300 and 6 pcs Al99.5-Globocer; at elevated temperature: 6 pcs Al99.5-SL150 and 6 pcs Al99.5-SL300). The aim of these tests was to determine how the MMSFs would perform as structural elements at higher temperature. The tests were performed and evaluated in accordance with the ruling standard about the compression tests of cellular materials [30].

4 Results and Discussion

The load bearing capacity of MMSFs depends on many parameters, such as the type and size of the microballoons, the test temperature, etc. In order to characterize these effects, we have done numerous compression tests as described in the previous section. During the tests, the engineering stress–engineering strain curves were plotted. The size of the hollow spheres has a detrimental effect on the compressive behaviour of MMSFs. The smaller hollow spheres (SL150 and SL300) ensured high compressive strength, but the first appearance of the fracture was sudden and quite rigid. For example, Fig. 2 shows the graph for an MMSF specimen containing small microballoons ($\text{\O}100\ \mu\text{m}$) tested at room temperature. Gupta *et al.* [31] and Bunn and Mottram [32] have investigated polymer matrix syntactic foams with similar stress–strain diagrams. According to the results of Gupta *et al.* the general stress–strain curves were divided into three parts [31]. Based on their idea, the diagram of MMSFs can be divided into three main parts containing overall five sections. In the first section (from point A to B) the specimens were deformed elastically only. In this section, the microballoons remained unharmed, as can be observed in Fig. 2a; there are no cracks at all. The overall deformation is related to the elastic deformation of the composite. The slope of the first part is defined as structural stiffness (S (MPa); see [30] about the standardized compression test of cellular materials). The stiffness is one of the characterizing properties of the MMSFs. In the vicinity of point A, the deviation from the fitted dashed line can be caused by the internal friction of the material or

by the springs of the tool and the natural friction of the sliding parts of the tool. Due to this, it should be distracted from the measured strain.

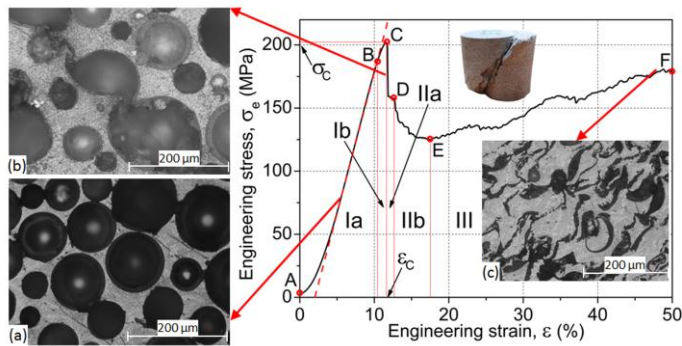


Figure 2

Typical compressive diagram of Al99.5-SL150-H/D=1.5 MMSF specimen

In the second section, from point B to C, the plastic deformation of the matrix began. The load transfer between the matrix and the microballoons increased to its maximum, but the microspheres remained still unharmed. At the end of this section, at point C, the stress reached the compressive strength (σ_c (MPa)) at the fracture strain (ϵ_c (%)). These parameters are also important characterizing properties, because they show the load bearing capacity of the MMSFs directly. At point C, the first crack appeared in the specimen. This first rupture was very thin and very sharp, and only one row of the microballoons was cracked, as is shown in Fig. 2b. The plane of the crack closed $\sim 45^\circ$ with the load direction, because in the case of uniaxial loading, the maximum shear load appears in this direction. The stress suddenly dropped to point D due to the reduced load bearing capacity caused by the fracture of the microballoons and the movement of the recently formed specimen halves. From point D to E, the fracture band expanded and the crack became thicker and thicker. The neighbouring microballoons broke and the load bearing capacity decreased further, but more slowly due to the friction between the specimen halves. This deformation phenomenon consumed significant strain and mechanical energy due to the fracture of the ceramic microballoons and due to the plastic deformation of the matrix. The absorbed specific mechanical energy (W (J/cm^3)) is the fourth main characterizing parameter of the MMSFs, as it indicates the damping and protecting capability of the MMSFs against a blast, collision or simple vibration. The absorbed specific energy is equal to the area under the recorded stress-strain curve and can be integrated numerically. From point E, the complete densification of the specimens took place. At the end of this process the cavities of the broken microballoons were filled by the matrix material due to its plastic deformation (Fig. 2c). This part, the plateau region, absorbs a lot of energy, because it is relatively long and has high stress value. The shape of the diagrams after point E can be ascending or constant (usually ascending because the densifying material needs higher force to

be deformed). It may contain larger drops or local peaks due to secondary cracks. The process ended at 50% engineering strain when the test stopped (F in Fig. 2).

Larger hollow spheres (Globocers with $\text{\O}1450 \mu\text{m}$) caused somewhat different behaviour during room temperature compressive tests (Fig. 3). The tracked properties were the same (compressive strength, fracture strain, structural stiffness and the absorbed specific energy), but the sudden drop in the force after the first stress peak was missing, so part IIa and IIb can be defined together as part IIa+b. The failure of the MMSFs was smoother, without large and sudden force drops. In Fig. 3a a cross section from the linear part is magnified; the hollow spheres are in good shape, and there is no sign of any crack. After the first stress peak, the hollow spheres began to crash (above the dashed line in Fig. 3b). At the end of the test the specimen were fully compacted, and only a few hollow spheres remained unharmed in the compression cone near to the surface of the tool (Fig. 3c).

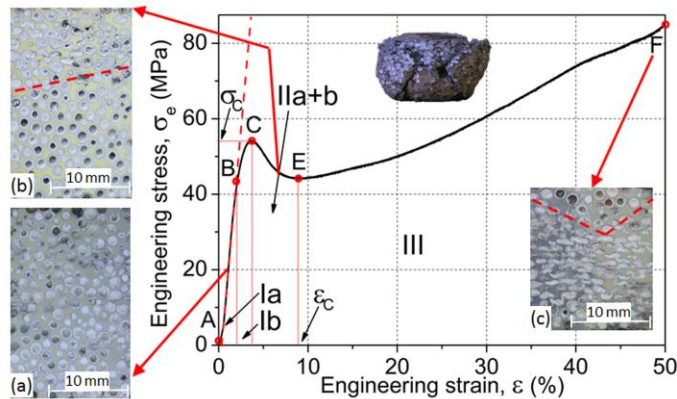


Figure 3

Typical compressive diagram of Al99.5-Globocer-H/D=1.5 MMSF specimen

The mechanical properties of the MMSFs can be characterized through the analysis of the above mentioned four material properties. The most important among them is the compressive strength, which is responsible for the load bearing capacity (Fig. 4).

The smaller hollow spheres ensured higher compressive strength than larger ones. This effect can be observed in the micrometer range also. The specimens containing smaller SL150 microballoons (average diameter $100 \mu\text{m}$) have about 10% higher compressive strength than the ones containing larger SL300 (average diameter $150 \mu\text{m}$) type microballoons. As shown in Table 2, the SL type microballoons are significantly smaller and they also have thinner wall. The smaller diameter and higher curvature give higher compressive strength and mechanical stability to the microballoons. Moreover, smaller wall thickness ensures lower probability for deflections; therefore the small SL type microballoons have higher compressive strength than the larger, Globocer type microballoons with thicker walls and more defects.

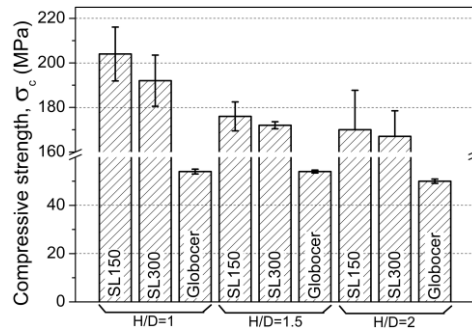


Figure 4

The effect of the microballoon size and aspect ratio on the compressive strength

Ceramics are especially sensitive for deflections; any small rupture or cavity can be the starting point of a crack. The effect of aspect ratio is also evident from Fig. 4. As the specimen height-specimen diameter ratio increased, the compressive strength decreased respectively. The MMSFs reinforced with smaller, SL type microballoons were more sensitive to this effect. In their case, the compressive strength drop is large (more than 30 MPa between $H/D=1$ and $H/D=2$), the specimens were buckled and shearing mode failure was observed even for specimens with $H/D=1.5$. In the case of bulky materials, this effect normally takes place if the aspect ratio is larger than 2.4. We can explain this phenomenon by the properties of the ceramic materials. They are quite sensitive to shear stresses; therefore, if there was any minimal shearing (due to not perfect specimen alignment for example), the negative effect of the shearing loading would be amplified by the sensitivity of the ceramic hollow spheres. The larger hollow spheres in the case of Globocer reinforced MMSFs were compressed rather than sheared, and therefore the aspect ratio has negligible effect on the compressive strength in this case; it remained almost constant with very narrow scatter. The next investigated property was the fracture strain (Fig. 5).

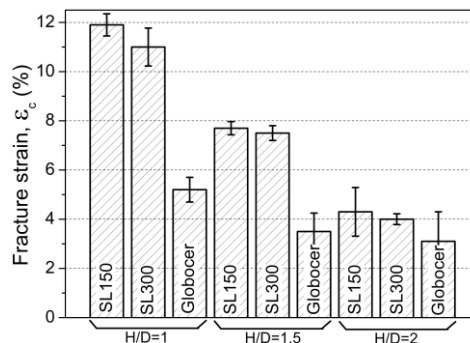


Figure 5

The effect of the microballoon size and aspect ratio on the fracture strain

The fracture strain showed similar behaviour as the compressive strength. The decrease in the strain was almost linear in the case of smaller hollow spheres, and larger spheres caused failure at smaller strains. These trends can be confirmed by the observation of the structural stiffness values (Fig. 6).

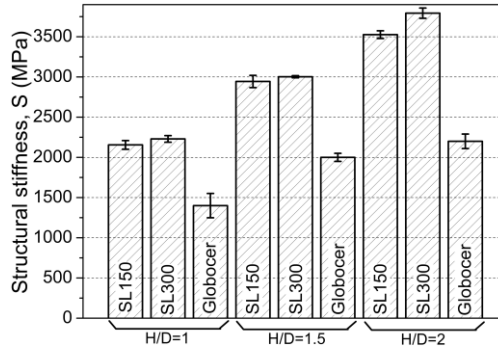


Figure 6

The effect of the microballoon size and aspect ratio on the structural stiffness

The initial slope of the plotted stress - strain curves increased linearly in all cases. The SL300 type reinforcement (larger microballoons) ensured higher structural stiffness than the smaller SL150 microballoon reinforcement, but the even larger Globocer type hollow spheres showed lower stiffness. This phenomenon can be explained by the different failure modes of the hollow spheres. The smaller ones were sheared and the larger ones were compressed. Finally, the consumed specific mechanical energies during the compressive tests are shown in Fig. 7.

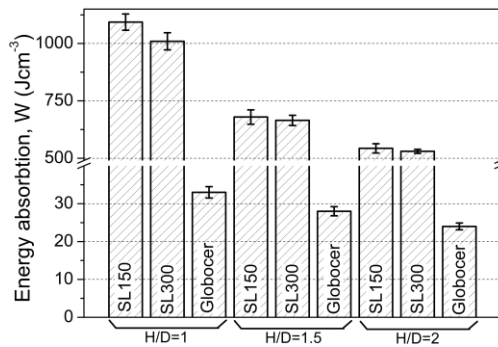


Figure 7

The effect of the microballoon size and aspect ratio on the consumed mechanical energy

As can be observed in Fig. 7, the consumed mechanical energy decreased significantly by the increment of the hollow spheres' size. Moreover the energy also decreased by the increasing aspect ratio. This phenomenon is indicated by the lower strength of the MMSFs. The lower compressive strength caused lower

plateau strength and, due to this, a smaller area under the compressive curve and lower consumed specific energy. This effect was more pronounced in the case of smaller hollow spheres; the H/D increment caused about 50% reduction in consumed energy. In the case of Globocer type hollow spheres, this reduction was only about 5-10%.

The influence of elevated test temperature is shown in Fig. 8 and presented by the example of SL type hollow spheres reinforced MMSFs.

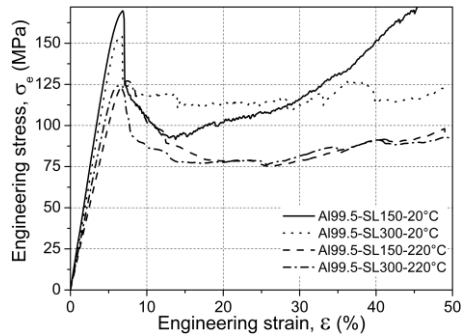


Figure 8

The effect of test temperature on the compressive behaviour of Al.995-SL300 MMSFs

In Fig. 8, the diagrams of the SL type hollow sphere reinforced MMSFs compressed at room and at elevated (220°C) temperature are shown and compared. Due to the elevated temperature, the compressive strength dropped by ~30-35%. In addition to this, the formability increased significantly, and due to this dual effect, the transmitted stress between the matrix and the hollow spheres increased slower than at room temperature and the first fracture appeared at higher strain. In short: the fracture strain increased by ~5% in all cases. The MMSFs became more ductile, but they remained strong enough and can be applied as structural elements: the compressive strengths were still above 120 MPa. This capability at elevated temperature is a serious advantage compared to the conventional metal and polymer foams and makes the MMSFs a good choice for structural parts in the neighbourhood of combustion engines or other heat producing systems. The absorbed specific energies were also decreased due to the lower compressive strength induced lower plateau strength. The effect of the microballoons' type was the same at elevated temperature too. The MMSFs with SL300 type microballoons showed ~5% lower compressive strength.

Conclusions

From the results of the above mentioned and discussed measurements the following conclusions can be drawn:

- The typical compression diagram of the MMSFs can be divided into three main parts containing five sections. The peak strength (compressive

strength), its strain (fracture strain), the structural stiffness and the area below the graph (the absorbed specific mechanical energy) can be applied as characterizing values of the compressive behaviour.

- The smaller, SL type microballoons ensured higher compressive strength, higher fracture strain and higher structural stiffness than the larger Globocer hollow spheres in all circumstances. In addition to the higher curvature and therefore higher compressive strength, the thinner wall of the smaller microballoons contains fewer defects than the thicker wall of the larger ones. The differences were significant between SL150 and SL300 microballoons too; again, the smaller SL150 type microballoons were stronger.
- The increased test temperature caused a ~30% drop in the compressive strength, while the fracture strain increased by ~5%. The structural stiffness decreased, and thus the MMSFs were more ductile than at room temperature. The decrease of compressive strength is significant but not too large; therefore, the MMSFs can be applied as structural elements at elevated temperatures.

In summary the compressive properties of MMSFs can be tailored by proper selection of the materials and by careful design for individual and unique applications.

Acknowledgement

The Metal Matrix Composites Laboratory is supported by Grant # GVOP 3.2.1-2004-04-0145/3.0. This paper was supported by the János Bolyai Research Scholarship of the Hungarian Academy of Sciences. The investigations were supported by The Hungarian Research Fund, NKTH-OTKA PD 83687. This work is connected to the scientific program of the " Development of quality-oriented and harmonized R+D+I strategy and functional model at BME" project. This project is supported by the New Széchenyi Plan (Project ID: TÁMOP-4.2.1/B-09/1/KMR-2010-0002). Thanks to C. H. Erbslöh Hungaria Ltd. and R. Tóth for providing the E-spheres.

References

- [1] Babcsán N, Leitmeier D, Banhart J: Metal Foams—High Temperature Colloids Part I. Ex Situ Analysis of Metal Foams. *Colloids and Surfaces A: Physicochemical and Engineering Aspects*. 2005;261(1-3):123-30
- [2] Babcsán N, Moreno FG, Banhart J: Metal Foams—High Temperature Colloids Part II: In Situ Analysis of Metal Foams. *Colloids and Surfaces A: Physicochemical and Engineering Aspects*. 2007;309(1-3):254-63
- [3] Erikson R: A Survey of Current Technology. 5th Aerospace Materials. Von Braun Center, Huntsville, Alabama 2002

-
- [4] Orbulov IN, Dobránszky J: Producing Metal Matrix Syntactic Foams by Pressure Infiltration. *Periodica Polytechnica Mechanical Engineering*. 2008;52(1):35-42
- [5] Sphere Services Inc, <http://www.sphereservices.com/>, last accessed: 6th December 2011
- [6] Enviropheres Ltd, <http://www.enviropheres.com/products.asp>, last accessed: 6th December 2011
- [7] Tudorache T, Popescu M: FEM Optimal Design of Wind Energy-based Heater. *Acta Polytechnica Hungarica*. 2009;6(2):55-70
- [8] Palmer R, Gao K, Doan T, Green L, Cavallaro G: Pressure Infiltrated Syntactic Foams—Process Development and Mechanical Properties. *Materials Science and Engineering: A*. 2007;464(1-2):85-92
- [9] Balch D, Odwyer J, Davis G, Cady C, Grayiii G, Dunand D: Plasticity and Damage in Aluminum Syntactic Foams Deformed under Dynamic and Quasi-Static Conditions. *Materials Science and Engineering A*. 2005;391(1-2):408-17
- [10] Balch D, Dunand D: Load Partitioning in Aluminum Syntactic Foams Containing Ceramic Microspheres. *Acta Materialia*. 2006;54(6):1501-11
- [11] Rohatgi PK, Guo RQ, Iksan H, Borchelt EJ, Asthana R: Pressure Infiltration Technique for Synthesis of Aluminum–Fly Ash Particulate Composite. *Materials Science and Engineering A*. 1998;244:22-30
- [12] Rohatgi P, Kim J, Gupta N, Alaraj S, Daoud A: Compressive Characteristics of A356/fly Ash Cenosphere Composites Synthesized by Pressure Infiltration Technique. *Composites Part A: Applied Science and Manufacturing*. 2006;37(3):430-7
- [13] Kiser M, He MY, Zok FW: The Mechanical Response of Ceramic Microballoon Reinforced Aluminum Matrix Composites under Compressive Loading. *Acta Materialia*. 1999;47(9):2685-94
- [14] Wu G, Dou Z, Sun D, Jiang L, Ding B, He B: Compression Behaviors of Cenosphere–Pure Aluminum Syntactic Foams. *Scripta Materialia*. 2007;56(3):221-4
- [15] Tao XF, Zhang LP, Zhao YY: Al Matrix Syntactic Foam Fabricated with Bimodal Ceramic Microspheres. *Materials & Design*. 2009;30(7):2732-6
- [16] Tao XF, Zhao YY: Compressive Behavior of Al Matrix Syntactic Foams Toughened with Al Particles. *Scripta Materialia*. 2009;61(5):461-4
- [17] Zhang LP, Zhao YY: Mechanical Response of Al Matrix Syntactic Foams Produced by Pressure Infiltration Casting. *Journal of Composite Materials*. 2007;41(17):2105-17
- [18] Mondal DP, Das S, Ramakrishnan N, Uday Bhasker K: Cenosphere-filled Aluminum Syntactic Foam Made through Stir-Casting Technique.

- Composites Part A: Applied Science and Manufacturing. 2009;40(3):279-88
- [19] Mondal DP, Das S, Jha N: Dry Sliding Wear Behaviour of Aluminum Syntactic Foam. *Materials & Design*. 2009;30(7):2563-8
- [20] Rabiei A, Oneill A: A Study on Processing of a Composite Metal Foam via Casting. *Materials Science and Engineering: A*. 2005;404(1-2):159-64
- [21] Ramachandra M, Radhakrishna K: Synthesis-Microstructure-Mechanical Properties-Wear and Corrosion Behavior of an Al-Si (12%)—Flyash Metal Matrix Composite. *Journal of Materials Science*. 2005;40(22):5989-97
- [22] Ramachandra M, Radhakrishna K: Effect of Reinforcement of Flyash on Sliding Wear, Slurry Erosive Wear and Corrosive Behavior of Aluminium Matrix Composite. *Wear*. 2007;262(11-12):1450-62
- [23] Couteau O, Dunand D: Creep of Aluminum Syntactic Foams. *Materials Science and Engineering: A*. 2008;488(1-2):573-9
- [24] Kuffová M, Nečas P: Fracture Mechanics Prevention: Comprehensive Approach-based Modelling? *Acta Polytechnica Hungarica*. 2010;7(5):5-17
- [25] Trumble KP: Spontaneous Infiltration of Non-Cylindrical Porosity Close Packed Spheres. *Acta Materialia*. 1998;46(7):2363-7
- [26] Barczy T, Kaptay G: Modelling the Infiltration of Liquid Metals unto Porous Ceramics. *Materials Science Forum*. 2005;473-474:297-302
- [27] Asthana R, Rohatgi PK, Tewari N: Infiltration Processing of Metal - Matrix Composites: a Review. *Processing of Advanced Materials*. 1992;2:1-17
- [28] Hollomet GmbH, <http://www.hollomet.com/cms/>, last accessed 28th November 2011
- [29] Jaeger HM, Nagel SR: Physics of the Granular State. *Science*. 1992;5051:1523-31
- [30] Testing of Metallic Materials - Compression Test of Metallic Cellular Materials, DIN50134 standard, October 2008
- [31] Gupta N, Kishore, Woldesenbet E, Sankaran S: Studies on Compressive Failure Features in Syntactic Foam Material. *Journal of Materials Science*. 2001;36:4485-91
- [32] Bunn P, Mottram JT: Manufacture and Compression Properties of Syntactic Foams. *Composites*. 1993;24(7):565-71